Progress In Electromagnetics Research C, Vol. 115, 81–93, 2021

Using a 3D Metamaterial to Enhance the Surface Wave Propagation for High Frequency Over-the-Horizon Radars: From Simulation to Outdoor Measurements

Quentin Herbette[1, 2, 3, *], Nicolas Bourey[4], Michel Menelle[1], Muriel Darces[2, 3], Stéphane Saillant[1], Yves Chatelon[2, 3], and Marc Hélier[2, 3]

Abstract—This article is about the characterization of a 3D metamaterial structure arranged to reinforce the surface wave radiation of antennas relevant to High Frequency (HF) surface wave radars. The use of a corrugated surface with a negative equivalent permittivity placed in the vicinity of the antenna increases the surface wave component of the radiated field. In order to confirm the anticipated performance of that metamaterial antenna, near-field measurements have been realized. Also, an original near far-field transformation technique, taking the surface wave into account, is applied to derive the radiation pattern of the antenna. Measurements were first achieved at reduced scale in UHF band and at full scale in HF band. At 1.1 GHz, they were operated on a small scale mock-up in a semi-anechoic chamber. An electric field acquisition setup installed in an Unmanned Aerial Vehicle (UAV) is used to characterize this antenna under outdoor conditions. This measuring system was especially designed for this application. The obtained results are discussed and enable us to validate the expected behavior of the antenna.

1. INTRODUCTION

Surface wave radars, which work in the HF band (between 3 and 30 MHz), have been used by ONERA since 2007. Such radars provide an economical and attractive alternative for the early detection of beyond-the-horizon targets. High Frequency Surface Wave Radar (HFSWR) is of particular interest for monitoring the Exclusive Economic Zone (EEZ). These radars are based on the ability of electromagnetic waves to propagate at the surface of the sea, allowing detections up to 215 nautical miles (400 km) [1, 2]. HFSWRs were previously integrated in the European Union research framework on Integrated Maritime Surveillance Systems (IMSS).

Antennas that are analogous to skywave radars are used for HFSWR, but the surface wave radiation of such antennas is limited [3]. Consequently, a study to enhance the surface wave radiation of these antennas has been started. The research began by investigating the requirements for launching a large surface wave. It has been demonstrated that a metamaterial with a negative permittivity would satisfy the required condition [4]. Original simulations and measurements at 1.1 GHz have been performed and indicate that a corrugated surface with a negative equivalent permittivity allows the presence of a larger surface wave. A real scale HF metamaterial was then manufactured. This structure is represented in Figure 1, and its size is: $21 \times 5 \times 2.5\,\mathrm{m}^3$. It was fabricated in stainless steel. The structure is placed on and connected to a wire mesh ground plane.

Received 17 June 2021, Accepted 26 August 2021, Scheduled 31 August 2021
* Corresponding author: Quentin Herbette (quentin.herbette@onera.fr).
[1] DEMR, ONERA, Université Paris Saclay F-91123 Palaiseau, France. [2] Sorbonne Université, CNRS, Laboratoire de Génie Electrique et Electronique de Paris, 75252, Paris, France. [3] Université Paris-Saclay, Centrale Supélec, CNRS, Laboratoire de Génie Electrique et Electronique de Paris, 91192, Gif-sur-Yvette, France. [4] Direction Générale de l'Armement, Information Superiority, Bruz, France.

Figure 1. 3D metamaterial designed for the HF band.

In the HF band as it will be explained later, far field measurements are difficult to perform. So, in order to characterize the field radiated by the structure in HF band, a near electric field measuring system embedded aboard a UAV has been developed. This original system allows to measure the near electric field in amplitude and phase [5]. A short preview of some results presented in this paper was previously released at the EuCAP 2021 conference in Düsseldorf [6]. A near to far-field transformation taking into account the ground electrical parameters and the surface wave propagation is applied here [7].

In Section 2, the concept of the proposed metamaterial is detailed. In Section 3, the UHF measuring system is depicted, and the data acquired at 1.1 GHz are displayed. In Section 4, the full-scale experimental results on the HF metamaterial are reported and commented. Last, a conclusion is drawn.

2. DESIGN OF THE METAMATERIAL AND FIRST VALIDATION

Figure 2 depicts the interface between two media, with the upper being air (permittivity ε_0 and permeability μ_0) and the lower being a lossy dielectric of electric conductivity σ and relative dielectric permittivity ε_{rr}. With ω being the angular frequency, the complex permittivity $\underline{\varepsilon_r}$ of medium 2 is written as follows:

$$\underline{\varepsilon_r} = \varepsilon_{rr} + \mathrm{j}\frac{\sigma}{\omega\varepsilon_0} \tag{1}$$

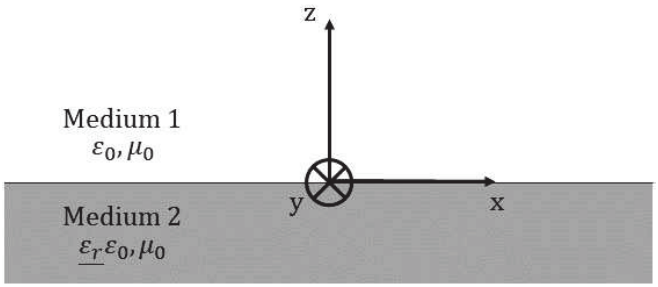

Figure 2. Interface between air (medium 1) and a lossy dielectric (medium 2).

It has been known since 2011 that an interface with negative permittivity can propagate and focus a lone surface wave. This demonstration has been performed with a field decomposition suggested by Kistovich [8]. To comply with the propagation requirements, it is needed to keep the relative permittivity below $\varepsilon_{rr} = -1$ and the conductivity as low as practically possible [9]. A periodic structure is employed to construct a metamaterial with such characteristics. That type of periodic structure is used in several

fields of operation, and their behavior has been extensively discussed in the scientific literature. The most common designs are corrugated surfaces, mushroom-shaped surfaces, and uniplanar surfaces.

These metamaterials have a frequency band gap in which the surface wave cannot propagate. In the bandwidth of the metamaterial, according to its geometry, the surface wave can be more or less strong and contained at the interface [10, 11].

During a preliminary study, with the intention of investigating the viability of such a metamaterial, the structure shown in figure (Figure 3(b)) has been fabricated. The chosen periodic structure is a corrugated surface which is able to guide an evanescent confined wave at ground level. It is made of a grounded dielectric slab supporting vertical parallel metallic walls [12]. The resulting periodical structure shows a regular arrangement of unit cells whose parameters are: d the length of a pattern which includes the thickness e of a plate, a the width of a groove between two nearby plates, and h the height of the walls. Such a structure can be seen in Figure 3 for which the excitation source is provided by a monopole antenna.

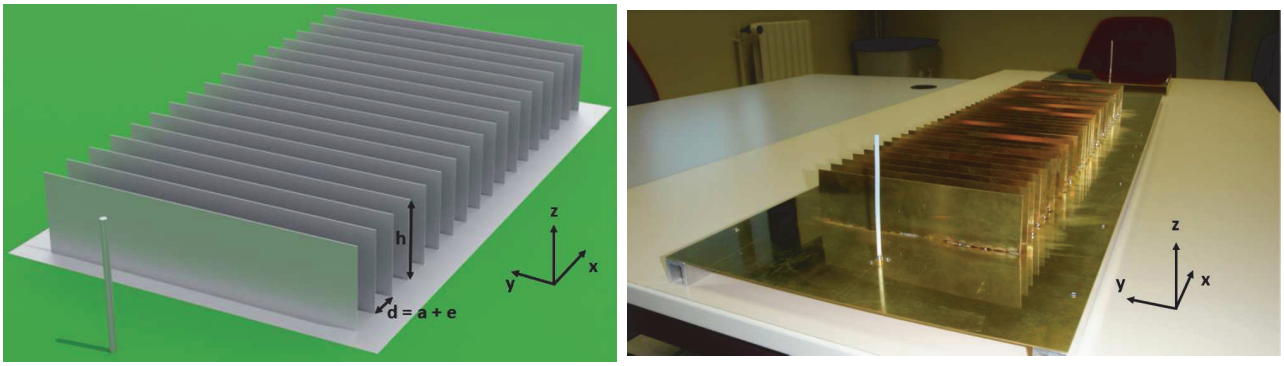

(a) (b)

Figure 3. (a) Geometry of the corrugated surface. (b) First metamaterial structure designed at 1.1 GHz.

It is necessary to optimize the geometrical parameters of the metamaterial to reach the desired performances. In order to determine those parameters, the dispersion relation for Transverse Magnetic (TM) confined waves is used under the assumption that $a < d \ll \lambda_0$ (the freespace wavelength) and that the length of the structure is infinite along the y-direction. It is given by [13]:

$$\sqrt{k_x^2 - k_0^2} = \frac{a}{d} k_0 \tan k_0 h \tag{2}$$

k_0 is the freespace wavenumber, and k_x is the wavenumber along the x-axis. Equation (2) tends to infinity for $k_0 = \frac{\pi}{2h}$ (or $h = \lambda/4$). As a consequence, since $k_z = \mathrm{j}\gamma = \mathrm{j}\sqrt{k_x^2 - k_0^2}$, with k_z the wavenumber along the z-axis, an extremely confined wave can be excited. The ratio $\frac{a}{d}$ must be as close to 1 as possible in order to have a panel thickness e as small as possible. This condition is necessary for the construction of the metamaterial structure. It is therefore required to modify the height h of the panels to maximize the magnitude of γ. In Figure 4, the propagation constant γ is plotted as a function of frequency for different values of h using Equation (2) and $\frac{a}{d} = 1.001$.

In the case of an evanescent confined wave, it has been shown that the wave number k_x can also be calculated from Equation (3) [9]:

$$k_x = k_0 \sqrt{\frac{\varepsilon_{rr}}{1 + \varepsilon_{rr}}} \tag{3}$$

The two full lines drawn in Figure 4 correspond to the derivation of γ using Equation (3) for different values of ε_{rr}. The intersection between these lines and the three curves drawn with Equation (2) gives the values of γ according to the expected operating frequency and ε_{rr}.

In order to validate the proper functioning of the structure and the existence of an actual wave confinement at the surface, the first validation was performed with an infrared thermography system

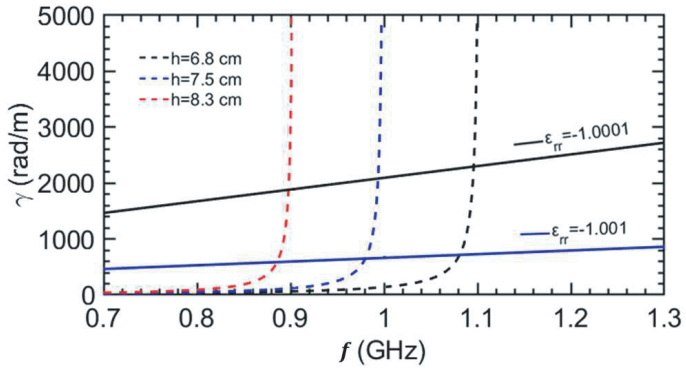

Figure 4. Application of Equation (2) for different values of h and Equation (3) for different values of ε_{rr}.

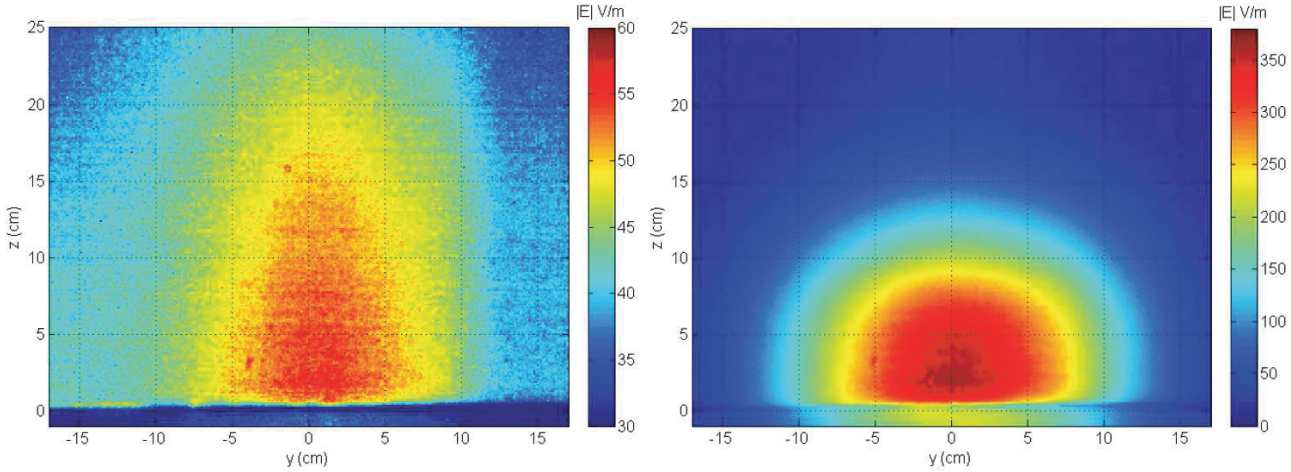

Figure 5. Measurement results obtained with EMIR technique at 1.1 GHz. (a) The monopole radiates alone above a PEC ground plane. (b) The monopole is associated with the corrugated structure.

developed by Onera and called the EMIR field imaging [14]. The results are presented in Figure 5. The first one corresponds to the magnitude of the vertical electric field radiated by the monopole alone (Figure 4(a)) and the second one to the amplitude of the field radiated by the monopole associated with the metamaterial (Figure 4(b)). We can notice that the amplitude of the electric field is greater at the interface with the ground plane when inserting the metamaterial, and the wave is focused.

3. SMALL-SCALE MEASUREMENTS

In order to directly measure the confinement of the wave at the interface, a semi-anechoic measurement bench operating in UHF band has been developed (Figure 6) [15]. This bench uses an electro-optic near-field probe, EFS-105 designed by enprobe [16], mounted on motorized rails which allow the displacement of the probe along 3 axes. Thanks to a two-port vector network analyzer, the complex transmission coefficient S_{21} is acquired. Port 1 feeds the Antenna Under Test (AUT), and port 2 is connected to the RF output of the probe base unit.

The magnitude of the measured electric field E_m is linked to the voltage V_m at port 2 with the probe antenna factor AF:

$$|E_m| = AF \cdot |V_m| \tag{4}$$

Using the antenna input power P_{in} and the impedance Z_2 of port 2, the power of the signal received

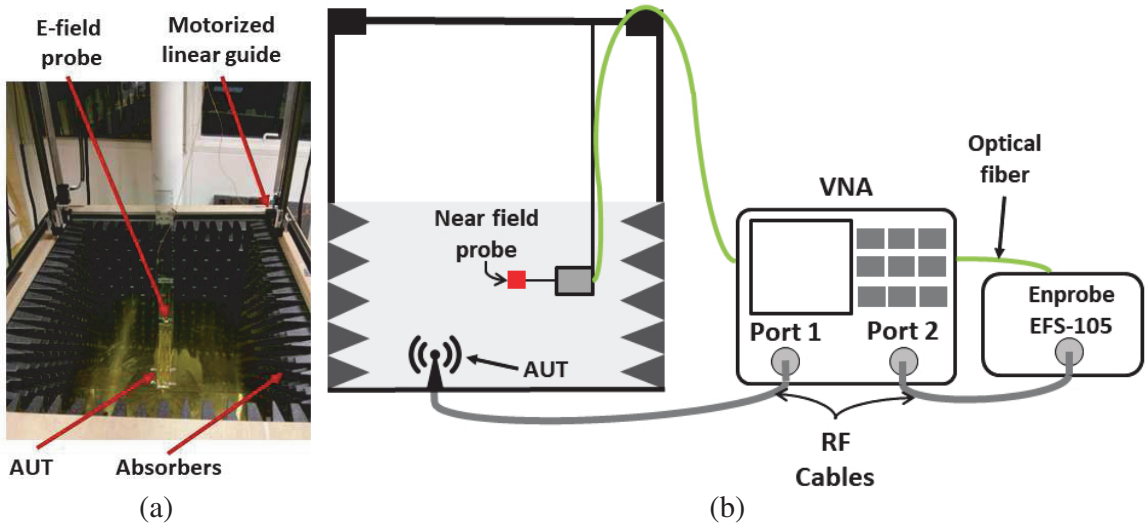

Figure 6. UHF semi-anechoic chamber and near-field bench.

at port 2 can be determined:

$$|S_{21}|^2 \cdot P_{in} = \frac{|V_m|^2}{Z_2} \tag{5}$$

Finally taking into account the delay δ brought by the optical fiber connecting the probe and the base unit, it is possible, using Equation (6), with f the working frequency, to determine the complex electric field E_m:

$$E_m = AF \cdot \sqrt{|S_{21}|^2 P_{in} Z_2} \cdot e^{\mathrm{j}(\angle S_{21} + 2\pi f \delta)} \tag{6}$$

By anticipating the necessity to reduce the load and the manufacturing costs of the HF structure, it has been decided to lighten the structure described in Section 2. For this purpose, the panels were opened up. The new structure, also called "open" structure and composed of three rows of 18 tabs, can be seen in Figure 7.

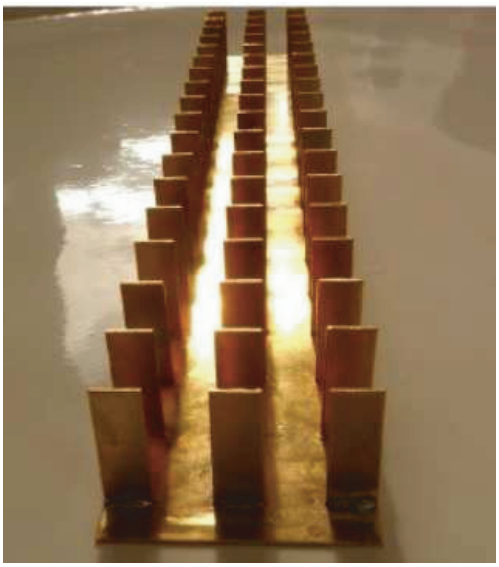

Figure 7. Lighter metamaterial structure designed at 1.1 GHz.

By measuring the field above the structure, the k_x wavenumber can be determined. Using Equation (3), the equivalent relative permittivity ε_{rr} of the structure can be derived at the frequency of 1.1 GHz. The value of the obtained permittivity is $\varepsilon_{rr} = -1.25$, which is in agreement with the expected value for a good confinement of the wave at the interface. As a performance indicator, the gain in electric field amplitude is measured at a distance of 745 mm ($\approx 2.5\lambda$) from the source. It is calculated using Equation (7). $Emeta_Z$ is the electric field radiated by the monopole combined with the structure, and E_Z is the electric field radiated by the monopole only:

$$G_e = 20 \log \left(\frac{|Emeta_Z|}{|E_Z|} \right) \tag{7}$$

At the end of the metamaterial, a gain about 10 dB is expected. In Figure 8 we can observe, from measurement in the longitudinal direction, the gain of the structure described in Section 2 (Figure 3(b)) compared to the lighter one (Figure 7). It is plotted according to height Z in millimeter which starts at zero at ground level. In the range of interest, i.e., at small heights, the difference between the two structures is small enough to favor using the lighter "open" structure.

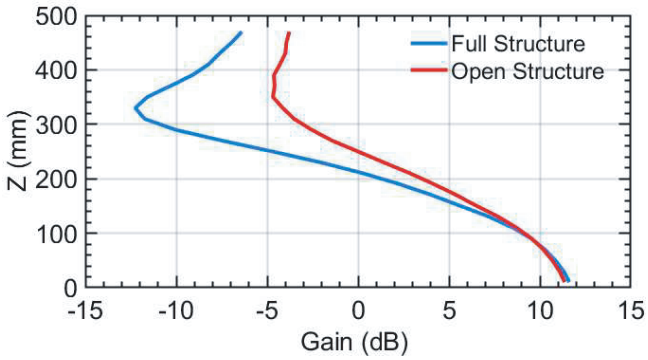

Figure 8. Gain obtained from measurement, for full and open structures at 1.1 GHz.

4. HF BAND MEASUREMENT

4.1. Near to Far Field Transformation

The main challenge of this work is to determine the radiation pattern of antennas in HF band. There are two major constraints in characterizing these antennas correctly. The first one is their huge size, and the second one is the impact of their close environment on the radiated field. Both issues prevent the use of classical characterization systems in an anechoic chamber. Also, due to the difficulty to fulfill the Fraunhofer distance condition for antenna arrays, far field measurements are impractical. A possible solution is therefore to perform a near field measurement and carry out a near to far-field transformation taking into account the surface wave propagation.

A source identification technique is used here for the near to far field transformation [7]. In order to carry out the transformation process, the three electric and three magnetic field components are required in amplitude and phase. To take into account all contributions of the field, i.e., the space wave, composed of the direct and reflected fields, and the surface wave, the radiation of the equivalent dipoles is analytically computed by means of Bannister's expressions [17]. The Bannister equations are based on Norton's work [18] and describe the radiation of a dipole placed above an infinite conducting plane. These formulas have the advantage of being applicable closer to the dipole. Using a plane wave approximation, the magnetic field can be determined from the electric field [7] which is therefore the only one evaluated. It is measured, in the near-field zone, on a surface S_M enclosing and centered on the antenna under test, as illustrated in Figure 9. The surface considered here is a cylinder of radius r_{SM} and height h_{SM}. At each surface measurement point, the electromagnetic field is the sum of all contributions from the dipoles. The equivalent sources are also placed on a virtual cylindrical surface,

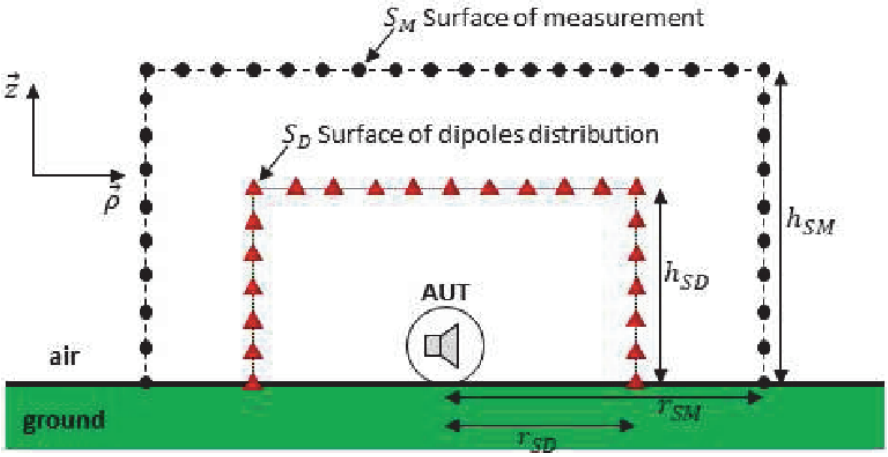

Figure 9. Near to far field transformation surfaces and antenna under test (AUT).

denoted as S_D, of radius r_{SD} and height h_{SD}. At each chosen point on S_D, three elementary electrical dipoles are orthogonally arranged.

4.2. Near Field Measuring System

The test measurements carried out at 1.1 GHz have shown the expected behaviour of the metamaterial. Therefore, a structure with the dimensions suited to the HF band has been developed (Figure 1). For its making, the difficulties encountered were the high cost of the raw material as well as the overall weight of the structure. It was therefore decided to reduce the number of panels from 18 to 13, resulting in a weight of the structure only about 8 metric tons and an expected gain G_e about 7 dB. To determine the correct operation of the latter at 15 MHz, it was necessary to design a near-field measurement system suited to outdoor tests. For this purpose, a dedicated measuring device embedded aboard a UAV has been developed and assembled to measure the electric field radiated by the full scale metamaterial antenna. This system is based on the same near electric field probe used in laboratory. The sensitivity of the near electric field probe EFS-105 is about $30\,\mu V/(m\sqrt{Hz})$.

In order to perform the near to far-field transformation, it is necessary to sample the complex electric field. The phase measurement is a hard task because a time synchronization between the transmission and the reception signals is required. For a frequency $f = 15$ MHz (i.e., a period $T = 66.66$ ns), accuracy on the phase shift of 10° is equivalent to the accuracy of less than 2 ns on the temporal shift. This challenge is the major restriction in the development of the measurement system.

The synchronization issue has been addressed by installing an optical fiber in the measuring system. With it, the information gathered by the near electric field probe is collected at ground level. In such a situation, a single clock can be used to digitize the transmitted and received signals. Other scientists, interested in using a UAV to analyze the radiation patterns of antennas, are implementing comparable solutions. The low weight of the optical fiber means that it has minimal impact on the payload. In addition, the optical fiber is insensitive to radio frequencies, making it resilient to any perturbation of the electric field information. A GNSS RTK positioning system has been incorporated into the drone. With this system, the accuracy on the drone positioning is less than 10 cm. Finally, it is required to move the probe away from the UAV to reduce the coupling effects between the characterized antenna and the drone. The distance to space the sensor and the drone was established using an electromagnetic simulation software. As the UAV manufacturer failed to provide the material physical properties of the drone, the simulation was carried out under the assumption of the worst case scenario, corresponding to a perfect electrical conductor (PEC) structure. To reduce the coupling in the HF band, the sensor must be placed at least 70 cm away from the drone, which is achieved using a fiberglass tube. The measurement system designed and installed on the drone is visible in Figure 10.

Figure 11 shows a block diagram explaining the measurement process. The local oscillator signal

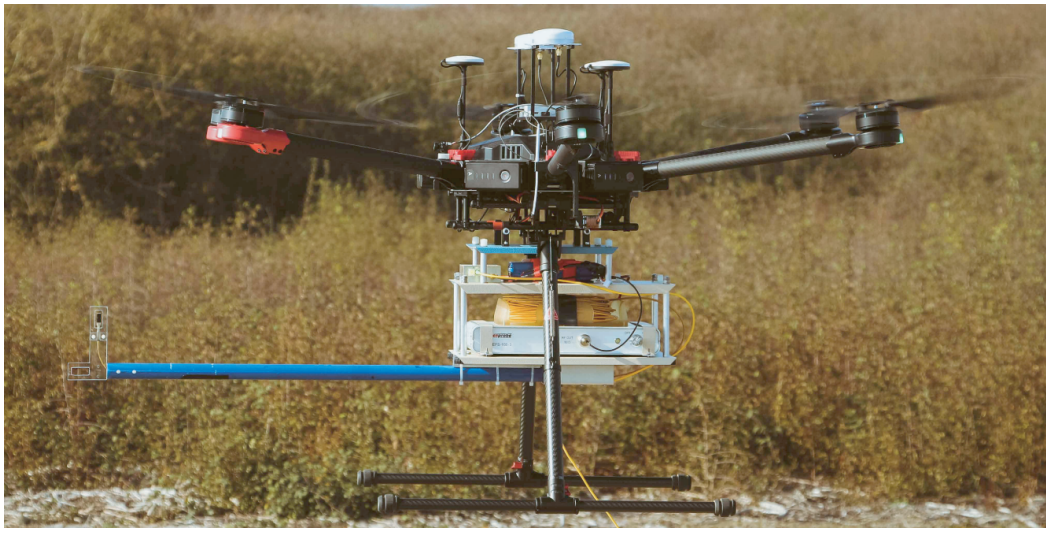

Figure 10. Measurement system aboard the UAV.

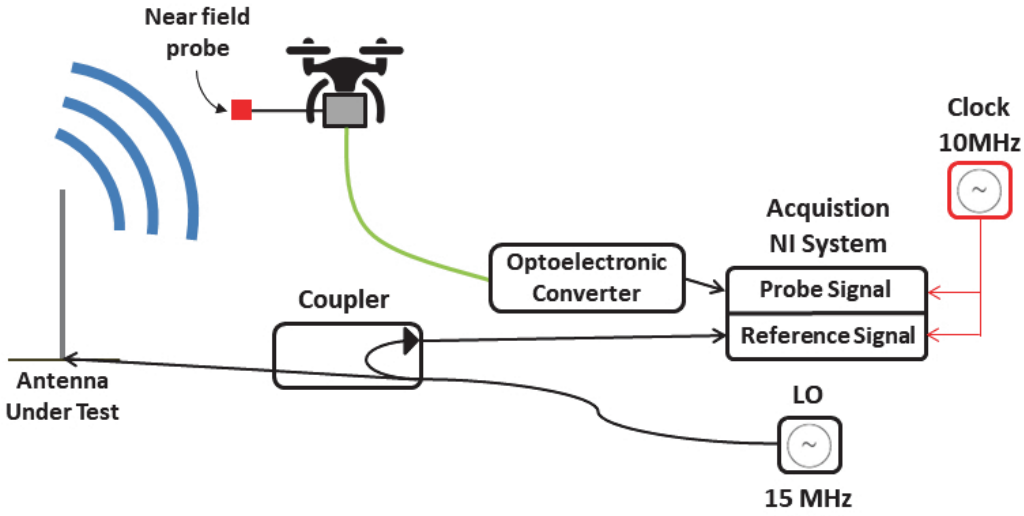

Figure 11. Block diagram of the antenna measurement set-up.

propagates through a coupler and part of it feeds the antenna under test. In this example, the excitation source was a monopole antenna. The data on the near electric field, provided by the probe, is transformed into a light signal by means of an onboard electro-optical converter. The signal is then converted back to an electrical signal at ground level using a long optical fiber and an optoelectronic converter. The signals, received and transmitted, are digitized, using the same clock, by a National Instruments digitizing system. The transmitted signal is used for the phase reference.

To characterize the metamaterial antenna, three kinds of measurement tracks were flown by the UAV. Figure 12(a) represents a set of horizontal flights over the structure to check the repeatability of the measurements, which are called "Test measurements". They are considered as reference measurements. The second type of measurement is illustrated in Figure 12(b), and it is made of horizontal measurements performed to map the field above the metamaterial allowing to display the wave confined at the interface. Lastly, to carry out the near to far field transformation, it is necessary to determine the field on the closed virtual surface S_M centred on the monopole. Figure 12(c) shows the vertical and radial lines that the UAV flies to define a corresponding closed cylindrical surface.

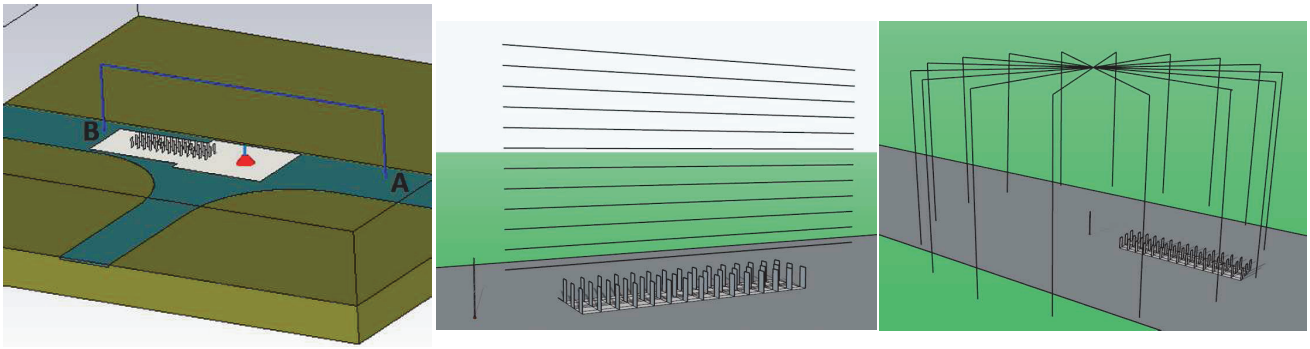

(a) (b) (c)

Figure 12. The three types of measurement paths.

4.3. Results Obtained in HF Band

To further confirm the experimental data, the operating environment was numerically modeled in a CST MWS electromagnetic simulation. In addition, because the ground on which the metamaterial antenna is located is heterogeneous, it has been modeled based on dielectric properties of concrete and soil [19, 20]. Using these simulations and test measurements, we were able to rapidly verify that the transmission system behaves as predicted. The blue path (AB) in Figure 12(a) is the UAV trajectory. The drone trajectory was accurately modeled in simulation in order to make comparisons with the actual measurements (point A corresponds to a curvilinear abscissa $s = 0\,\text{m}$ and point B to $s = 115\,\text{m}$). As shown in Figure 13, there is a strong match between measurements and simulations on the vertical component of the electric field, both in magnitude and phase. For an equal distance away from the monopole, the field radiated by the structure is found to be greater at the extremity of the metamaterial. Comparable conclusions could be drawn for the radial component of the electric field. It was confirmed that the electric field's azimuthal component was insignificant, as anticipated. It was therefore not captured for the remaining measurements.

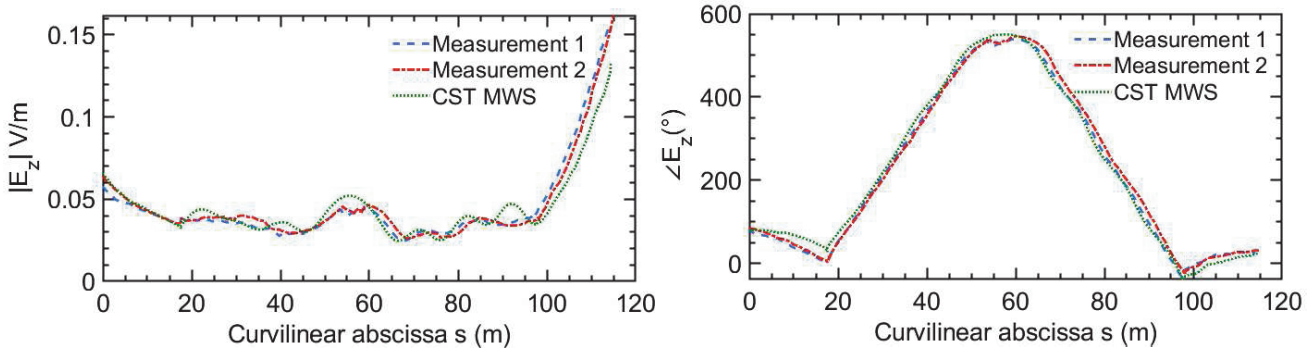

(a) (b)

Figure 13. Test measurements — Amplitude and phase of the vertical electric field: comparison between measurements and simulations.

The next group of results are derived from the measurements along the horizontal paths. To evaluate the bandwidth of the metamaterial structure, 8 measurements at different frequencies were performed. Figure 14(a) displays the data for three of the measurements. The simulations results for a similar environment are shown in Figure 14(b). One can observe that the vertical distributions of the electric field for the measurement and simulation are similar for all the three frequencies. The interpolation algorithm employed to produce field maps from the lines leads to some variations in the

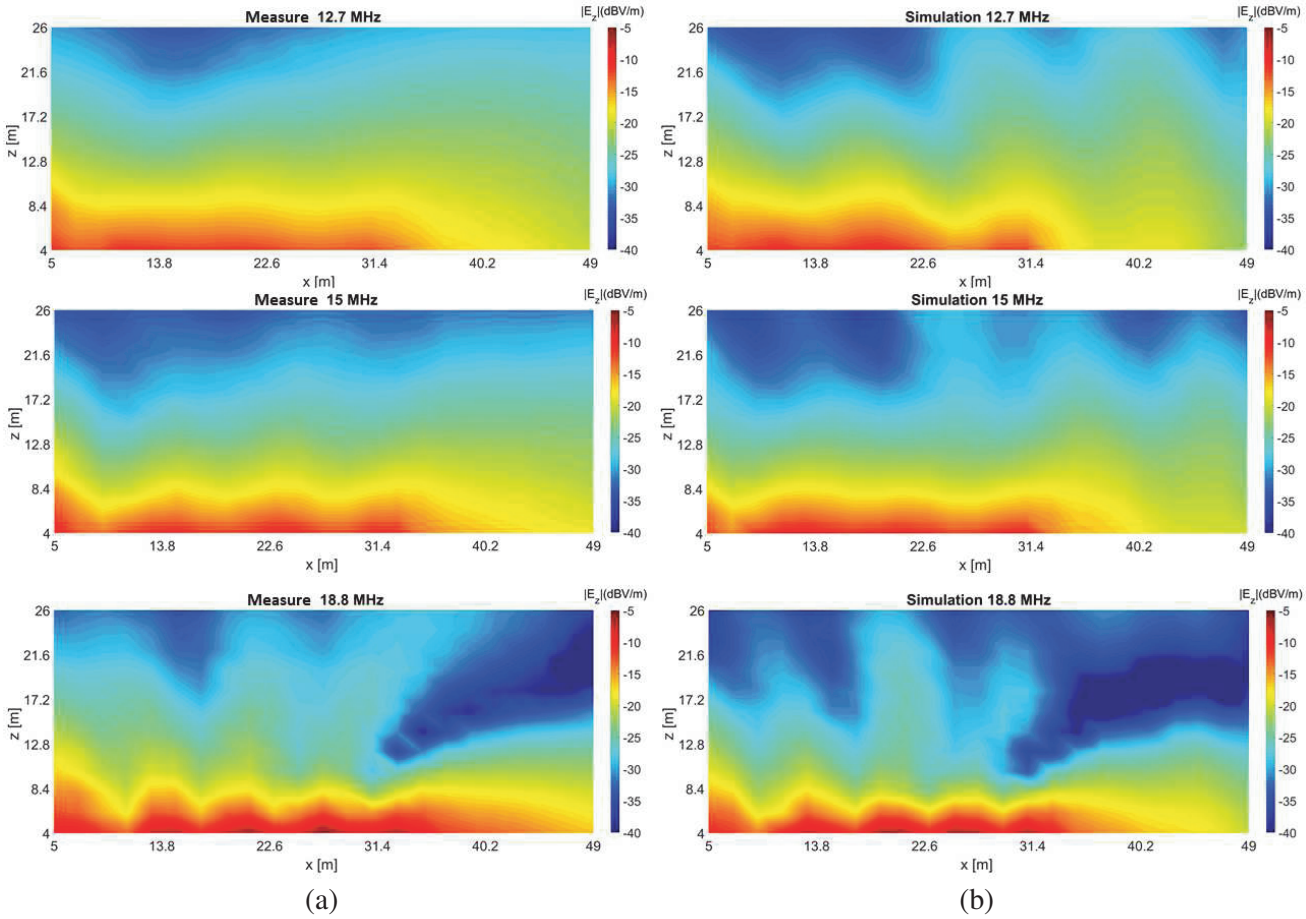

Figure 14. Horizontal lines — Amplitude of E_z component: (a) measurements at 12.7 MHz, 15 MHz and 18.8 MHz, (b) simulations at 12.7 MHz, 15 MHz and 18.8 MHz.

Table 1. Root mean squared errors for the three frequencies.

Frequency (MHz)	RMSE (dBV/m)
12.7	−38.4
15	−36.7
18.8	−30.6

density plots. The root mean squared errors for the three frequencies have been evaluated and are presented in Table 1. These error levels are about 10 dB lower than the average amplitude of the observed fields.

The good confinement of the wave at ground level can be noted. By observing the figures, it might appear that the structure, dimensioned for 15 MHz, shows better performances at 18.8 MHz. However, the target application is the radar one, with an azimuthal main lobe opening of about 30° and a strong reduction of the field radiated towards the ionosphere. These different features are missing at the frequency of 18.8 MHz. In addition, from these measurements it was possible to derive the wavelength λ_x in the propagation direction and, using Equation (3), to determine the equivalent permittivity of the metamaterial for the different frequencies (Table 2). Those results are close to $\varepsilon_{rr} = -1$ which fulfils the condition to radiate a strong surface wave.

The last results are obtained using the cylindrical paths and allow to carry out the near to far-field

Table 2. Measured wavelength above the metamaterial and equivalent permittivity.

Frequency (MHz)	λ_x (m)	ε_{rr}
12.7	10.5	-1.25
15	9.2	-1.26
18.8	8.5	-1.39

transformation. Two measurements, one per component (radial E_ρ and vertical E_z), were performed with the following parameters: $h_{SM} = r_{SM} = 2\lambda = 40\,\text{m}$. The azimuthal $\Delta\phi$ step for each vertical generatrix was 15°. A total duration of 40 minutes per component were needed to scan the cylinder. The points described by the drone during the measurement of the radial and vertical components of the electric field are plotted in Figure 15. The reproducibility of the paths, even for complex geometry, is noticeable.

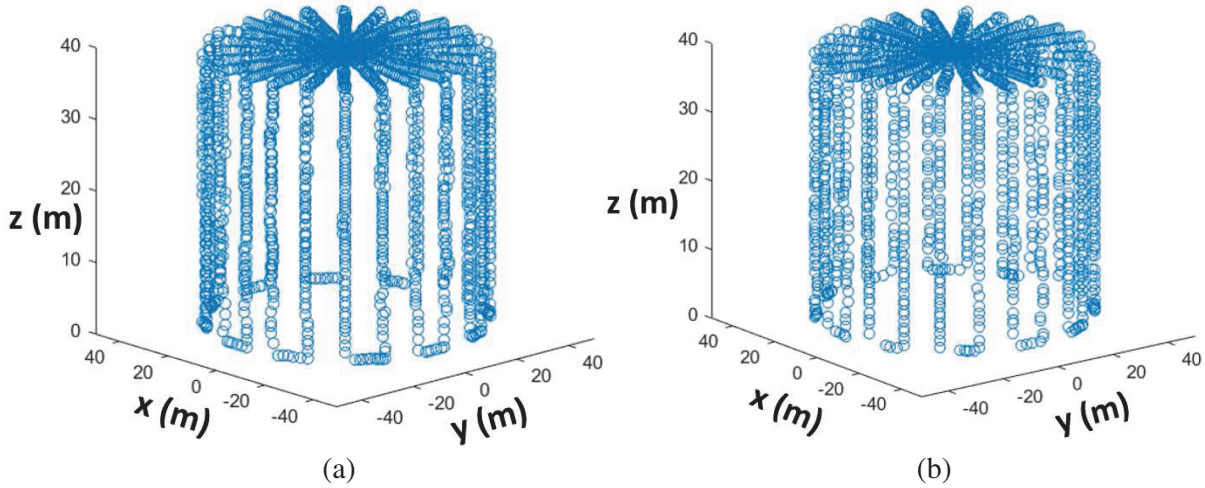

Figure 15. Measurement cylinders chosen for (a) E_ρ, (b) E_z.

The measurements are carried out in a continuous way which leads to a large number of samples to process. To perform the near to far-field transformation, only 24 equispaced points at $\lambda/6$ were selected for each vertical generatrix. This decimation was suitable to generate a cylinder of equivalent sources applying the method presented in Section 3. The dimensions of the dipoles cylinder are

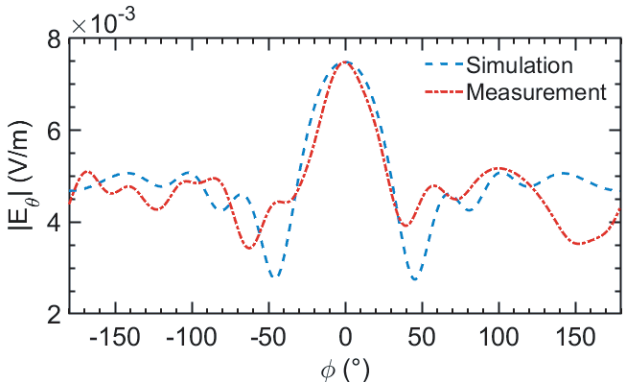

Figure 16. Far-field evaluated at 300 m from the antenna for measurement and simulation.

$h_{SD} = r_{SD} = 30$ m. The dipoles are arranged every $3\lambda/16$, and the $\Delta\phi$ step for each generatrix is 22.5°. The transformation algorithm allows to calculate the field radiated by the antenna at 300 m on a ground considered as soil. In the light of the difficulty of measuring the field radiated by the antenna at large distance, the validation is carried out with respect to the simulation illustrated in Figure 12(a). The far field results, from measurement and simulation, are plotted in Figure 16 and are in good agreement. The far field magnitude determined from the measurements has a similar shape to the one determined from simulation. The main differences seem to be due to errors on the measured phase at some critical points for the near to far-field transformation algorithm.

5. CONCLUSION

Firstly, a reduced scale mock-up of a metamaterial antenna, transmitting around 1.1 GHz, has been fabricated. The comparison performed between the measured near electric field and the simulated one shows a good agreement between them. Then, the HF full scale metamaterial antenna has been built, and its near electric field is characterized by means of a UAV specially instrumented for that purpose. Again, the measured results are in good agreement with the simulated ones. This has resulted in the deployment of the metamaterial antenna inside an actual operating radar system temporarily installed on the French coast of the Mediterranean Sea whose first results will be soon analyzed.

ACKNOWLEDGMENT

DGA (French Ministry of Defense) is thanked for its contractual contribution to the RAPID AC3M program in which both the metamaterial and the airborne system were defined and deployed.

REFERENCES

1. Ponsford, A., "Surveillance of the 200 nautical mile Exclusive Economic Zone (EEZ) using High Frequency Surface Wave Radar (HFSWR)," *Canadian Journal of Remote Sensing*, Vol. 27, No. 4, 354–360, 2001.
2. Vesecky, J. F., K. E. Laws, and J. D. Paduan, "Using HF surface wave radar and the ship Automatic Identification System (AIS) to monitor coastal vessels," *2009 IEEE International Geoscience and Remote Sensing Symposium*, Vol. 3, III-761–III-764, 2009.
3. Jangal, F. and M. Menelle, "French HFSWR contribution to the European integrated maritime surveillance system I2C," *IET International Radar Conference 2015*, 1–5, Oct. 2015.
4. Petrillo, L., F. Jangal, M. Darces, J.-L. Montmagnon, and M. Hélier, "Towards a better excitation of the surface wave," *Progress In Electromagnetics Research M*, Vol. 13, 17–28, 2010.
5. Herbette, Q., S. Saillant, M. Menelle, B. Urbani, N. Bourey, M. Darces, and M. Hélier, "HF Radar antenna near field assessment using a UAV," *2019 International Radar Conference (RADAR)*, 1–4, Sept. 2019.
6. Herbette, Q., N. Bourey, M. Menelle, M. Darces, S. Saillant, and M. Hélier, "Using a 3D metamaterial to enhance surface wave propagation in HF band," *2021 15th European Conference on Antennas and Propagation (EuCAP)*, 1–5, Mar. 2021.
7. Payet, N., M. Darces, J.-L. Montmagnon, M. Hélier, and F. Jangal, "Near field to far field transformation by using equivalent sources in HF band," *2012 15 International Symposium on Antenna Technology and Applied Electromagnetics*, 1–4, Jun. 2012.
8. Kistovich, Y. V., "On the possibility of observing surface zenneck waves in the radiation of a source with a small vertical aperture," *Journal of Technical Physics*, Vol. 59, No. 4, 16–21, 1989.
9. Jangal, F., L. Petrillo, M. Darces, M. Hélier, and J.-L. Montmagnon, "Inductive surface element," Patent: EP2888784B1, Jul. 2015.
10. Elliott, R., "On the theory of corrugated plane surfaces," *Transactions of the IRE Professional Group on Antennas and Propagation*, Vol. 2, No. 2, 71–81, 1954.

11. Yang, F. and Y. Rahmat-Samii, *Electromagnetic Band Gap Structures in Antenna Engineering*, The Cambridge RF and Microwave Engineering Series, Cambridge University Press, 2008.
12. Rotman, W., "A study of single-surface corrugated guides," *Proceedings of the IRE*, Vol. 39, 952–959, Aug. 1951.
13. Garcia-Vidal, F. J., L. Martín-Moreno, and J. B. Pendry, "Surfaces with holes in them: New plasmonic metamaterials," *Journal of Optics A: Pure and Applied Optics*, Vol. 7, S97–S101, Jan. 2005.
14. Balageas, D. and P. Levesque, "EMIR: A photothermal tool for electromagnetic phenomena characterization," *Revue Générale de Thermique*, Vol. 37, 725–739, Sept. 1998.
15. Bourey, N., M. Darces, and M. Hélier, "In situ antenna far field estimation based on equivalent sources," *2018 USNC-URSI Radio Science Meeting (Joint with AP-S Symposium)*, 105–106, Jul. 2018.
16. Kortke, A. and W. Mann, "Near field scanning with optoelectronic e-field probes," *2009 3rd European Conference on Antennas and Propagation*, 1725–1729, 2009.
17. Bannister, P. R., "New formulas that extend Norton's farfield elementary dipole equations to the quasi-nearfield range," 1984.
18. Norton, K. A., "The propagation of radio waves over the surface of the earth and in the upper atmosphere," *Proceedings of the Institute of Radio Engineers*, Vol. 25, No. 9, 1203–1236, 1937.
19. Bourdi, T., J. E. Rhazi, F. Boone, and G. Ballivy, "Application of Jonscher model for the characterization of the dielectric permittivity of concrete," *Journal of Physics D: Applied Physics*, Vol. 41, 205–210, Oct. 2008.
20. Loewer, M., J. Igel, C. Minnich, and N. Wagner, "Electrical and dielectric properties of soils in the mHz to GHz frequency range," *Proceedings of the 11th International Conference on Electromagnetic Wave Interaction with Water and Moist Substances (ISEMA)*, 247–254, 2016.